

Comparison of Different Synthesis Ways for Mg–Al- Layered Double Hydroxides (LDH), Effects of Ultrasound Treatment and Characterization of the Structural Phases by Rietveld Refinement

Salem. Babay*, Mohamed Toumi

Laboratory of the Physico-Chemistry of Solid States, LR11 ES51, University of Sfax, Road of Soukra km 4, Sfax3038, Tunisia

*Corresponding author: Salem. Babay, Laboratory of the Physico-Chemistry of Solid States, LR11 ES51, University of Sfax, Road of Soukra, Tunisia, Tel : (+216) 90122344 ; E-mail: salem.babay@yahoo.fr

Abstract

Layered Double Hydroxides (LDH) with carbonate as interlayer anion and an Mg^{2+}/Al^{3+} ratio of 3 (also denoted as Mg–Al–CO₃–LDHs in this paper), were synthesized based on the coprecipitation method under different synthesis conditions: under ultrasound treatment and without ultrasound treatment. The effects of ultrasound irradiation on the structural, textural and sorption behavior of fluoride ion from contaminated water by the LDH products were studied, resulting in higher basal spacing's, smaller crystallite size and higher removal efficiency of fluoride in contaminated water compared to an Mg–Al layered double hydroxides prepared without sonication. The material of Mg–Al–CO₃, molar ratio Mg: Al of 3 prepared by conventional method of co-precipitation without ultrasound treatment is characterized by Rietveld refinement of the X-ray powder diffraction pattern, DTA-TGA, Infrared and Raman spectroscopies. The thermal behavior of synthetic hydrotalcite is studied by heating stage Raman microscopy and heating stage of X-ray powder diffraction. The decomposition of this hydrotalcite-like structure on heating up to 600°C yields a mixture of two phases: a percales MgO phase and a spinal-like phase of MgAl₂O₄, which is also tested in the removal of fluoride in contaminated water, and which has higher removal efficiency (64.5%).

Keywords: Inorganic compounds, Mg–Al LDH, Ultrasound treatment, Rietveld, X-Ray diffraction, Infrared spectroscopy, Thermal decomposition; Mixed oxides, Fluoride removal

Received date: September 16, 2017

Accepted date: December 5, 2017

Published date: December 12, 2017

Citation: Babay, S. et al. Comparison of Different Synthesis Ways for Mg–Al- Layered Double Hydroxides (LDH), Effects Of Ultrasound Treatment and Characterization of the Structural Phases By Rietveld Refinement. (2017) J Nanotechnol Mater Sci 4(2): 112- 120.

DOI: 10.15436/2377-1372.17.1688



Introduction

Layered Double Hydroxides (LDH), anionic clays, is a family of compounds which have attracted considerable attention in recent years^[1-4] such as catalysis^[5], adsorption^[6], ion exchange^[7], biomedical application^[8] and Defluoridation Capacity (DC)^[9].

The structure of most of these materials corresponds to that of hydrotalcite^[10]. LDHs are characterized by the general formula $[M^{II}_{1-x}M^{III}_x(OH)_2]^{x+}[X_{n/x}^{n-}m H_2O]^{x-}$, symbolized by $[M^{II}-M^{III}-X^{n-}]$, where M^{II} and M^{III} are the di- and trivalent cations and Xⁿ⁻ is an exchangeable interlayer anion, notably (carbonate, nitrate, halides, complexes anions, oxo-anion, etc.)^[11,12].

A large number of LDH are a combination with divalent

cations, for instance Mg²⁺, Mn²⁺, Fe²⁺, Co²⁺, Ni²⁺, Cu²⁺, Zn²⁺ and trivalent cations, namely Al³⁺, Cr³⁺, Mn³⁺, Fe³⁺, Co³⁺, La³⁺^[13,14]. The charge density on the layers of the LDH will clearly depend upon the M^{II} / M^{III} ratio which usually lies between 2 and 4^[15].

For synthesizing LDH, several methods are described, such as the hydrothermal route^[16], anionic exchange method^[17], and coprecipitation method^[18]. Amongst these methods, the coprecipitation in aqueous solution is the most common method for LDH synthesis^[19]. The benefit of this method is that several synthesis parameters can be controlled independently during the precipitation process^[19,20]. Recently, hydrotalcite composite received attention in the domain of water treatment^[21]. Those



Hydrotalcite-like compound, also known as Layered Double Hydroxides (LDH), constitute an important class of inorganic materials with desirable properties to remove anionic pollutants from water^[22,23]. The presence of sizable interlayer spaces and large quantity of exchangeable anions, make LDH compound and their calcined products excellent adsorbents for the removal of toxic anions from contaminated waters^[24-26].

Fluoride contamination in drinking water, due to natural and anthropogenic activities, has been recognized as one of the major problems worldwide imposing a serious threat to Human health^[27]. Drinking water is the single major source of fluoride intake which, when consumed in excess, may lead to various diseases, especially osteoporosis, arthritis, cancer, brain damage, Alzheimer syndrome and thyroid disorder^[28,29]. Among several treatment technologies applied for Fluoride removal, there are various methods have been suggested to reduce the fluoride concentration in water, for instance, precipitation, ion exchange, filtration adsorption by LDH product^[30-34]. However, to our knowledge, the performance of as-synthesized LDH prepared under ultrasound irradiation in the defluoridation of water has not yet been reported. In fact the present work deals with the preparation of carbonate – intercalated, Mg-Al, LDHs by co precipitation method at constant p H and examines the effect of ultrasound treatment on the structural, textural and sorption behavior of fluoride anion from contaminated water by the LDH products. This study also investigates the thermal decomposition of Mg-Al LDH_{s1} prepared without ultrasound treatment.

Experimental

Preparation of [Mg-Al-CO₃]

Mg–Al–CO₃–LDH_{s1}; with Mg/Al ratio 3.00 was synthesized by coprecipitation method at constant pH. A solution of Mg Cl₂ 6H₂O (0.75 M) and Al (Cl)₃ 9H₂O (0.25 M) in 80 ml of distilled water was dropwise added at a constant rate (about 1 ml/min) at room temperature to 100 ml of aqueous solution containing 0.35 mol of NaOH and 0.09 mol of Na₂CO₃. The pH was maintained constant (pH = 10) by the drop wise addition of aqueous solution of NaOH (1 mol/l). Once the addition was completed, the solution was maintained at 75°C for 48h. The suspension was filtered, washed several times with distilled water, and then dried at room temperature and at 105°C for 18h.

The conventional synthesis of Mg–Al–CO₃–LDH_{s2} under ultrasound treatment was carried out following the same procedure as mentioned above without ultrasound treatment: Mg–Al–CO₃–LDH_{s1} (at constant pH and composition ratio of Mg and Al was also the same as described above), then the suspension was conducted for 3 hours by ultrasound instruments.

The amplitude of the ultrasonic waves and pulses were set as follows:

- Amplitude of ultrasonic waves: 50%
- Pulse: 2 sec on; 1 sec off.

The suspension was filtered, washed several times with distilled water, and then dried at room temperature and at 105°C for 18h.

Adsorption of fluoride

The experimental procedure is carried out as follows: 0.1 g of the compound LDH prepared under ultrasound treatment (LDH_{s2}), calcined layered double hydroxides CLDH and

the sample, prepared without ultrasound treatment (LDH_{s1}), are suspended each in a solution of NaF(10 mg/l). The pH of the solution is adjusted at 7 using 0.01M HCl and/or NaOH. The solution is stirred at room temperature (25°C). Afterwards; the concentration of fluoride is determined by a specific probe (wtw ino Lab series Ph / ion745) at times t defined. We can determine the concentration of fluoride removed by mass of the compound. The amount of fluoride (Q_e) and removal efficiency (E) are calculated using the Following equations:

$$Q_e = ((C_0 - C_e) / m) \times V$$

$$E = Q_e \times 100$$

Where Q_e is the amount of fluoride adsorbed per unit, the mass of the adsorbent at equilibrium (mg / g), C₀ is the initial concentration of fluoride ion in the solution (mg.L⁻¹) and C_e is the equilibrium concentration of fluoride ion in the solution (mg.L⁻¹). V is the volume of the solution in contact with the adsorbents (L), m is the weight of the adsorbent used in the experiment (LDH_{s1}, CLDH or LDH_{s2}) (g) and E is the removal efficiency (%).

Structural characterisation techniques

X-Ray diffraction

Powder X-Ray Diffraction (PXRD) patterns are determined on a P analytical X' Pert PRO MPD powder X-ray diffractometer equipped with an X'cellerator detector operating with a secondary monochromator and using a CuK α radiation source (K α_1 = 1.5406 Å and K α_2 = 1.5444 Å). The diffraction pattern was recorded under ambient atmosphere over an angular range of 5 - 120° (2 θ), with a step length of 0.017° (2 θ) and a counting time of 27.5.s step⁻¹. Each of the powder diffraction patterns confirmed that the synthetic compound was formed by rhombohedra symmetry, hydrotalcite -type phase (space group).

Infrared spectroscopy

The Infrared (IR) absorption spectrum was carried out on a pellet sample prepared by mixing 1.0 mg sample for a total weight (samples + KBr) of 200 mg. The spectrum was obtained on a Perkin-Elmer FT-IR system PC spectrophotometer (at the University of Sfax) in the 4000 – 400 cm⁻¹ range (30 scans) with 2 cm⁻¹ spectral resolution. A 200 mg KBr pellet was used as reference to correct the background.

DTA-TGA analysis

In order to estimate the interlayer water content, thermo gravimetric (TGA) and Differential Thermal Analysis (DTA) were performed using a thermal analyzer (SDT Q600 V8.1 Build 99, TA instrument). Curves were recorded at room temperature up to 800°C at a rate of 10°C/min and using 13.66 mg of the sample, which was initially in equilibrium with this air flow.

Heating stage Raman spectroscopy

The Raman spectra were recorded at room temperature in the backscattering configuration on a T64000 Jobin-Yvon-Horiba spectrometer equipped with the diffraction grating 600 lines/ mm under a microscope (Olympus Bx41) with a 100× objective focusing on the 514 nm line from an argon–krypton ion laser (coherent, Innova). The spot size of the laser was estimated at 0.8 μm and the spectral resolution at 2 cm⁻¹.

The samples were isothermally annealed at different temperatures (50, 100, 150, 230, 280, 320, 360, 400, 440, 500, 550 and 600 °C).

Results and discussion

Characterization of [Mg–Al–CO₃²⁻]

Structural characteristics

Effect of ultrasound treatment

The XRD patterns for the resulting solids are shown in Figure 1. For comparison, the XRD patterns for the LDH synthesized in a conventional constant- pH process are also illustrated. In each case, The XRD patterns exhibit the characteristic reflections corresponding to the (003), (006), (009) and (110) planes for Mg–Al–CO₃–LDH_s, respectively, indicating the formation of mostly well-crystallized hydroxalcalite-like phase indexed to typical carbonate hydroxalcalite structure with the rhombohedra system with the $R\bar{3}m$ space group (JCPDS 22-700).

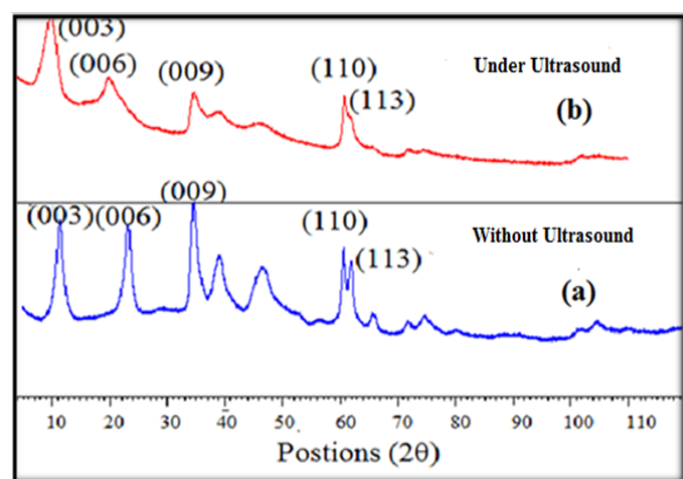


Figure-1: The XRD patterns for the LDH synthesized in a conventional constant- pH process.

- (a): Without Ultrasound treatment (Mg–Al–CO₃ LDH_{s1})
 (b): Under Ultrasound treatment (Mg–Al–CO₃ LDH_{s2})

For LDH synthesized under ultrasound treatment (Mg–Al–CO₃–LDH_{s2}), the reflection intensity decreases while the half width increases relative to that prepared by a constant pH without sonication, indicating smaller LDH crystallites or inhibited crystallization in the former process. The broadening of the (110) reflection around 60° indicated some disorder in the structure, which was directly related to a reduced aggregation of the particles during sonication. The XRD pattern of each prepared sample was analyzed by the Rietveld method, using the pattern matching routine of the Fullprof program^[35] integrated in Winploter software^[36]. The detailed structural parameters for the Mg–Al–CO₃–LDHs under different conditions are listed in Table 1. The crystallite size of Mg–Al–CO₃ LDHs like- phase prepared by different methods can be calculated using Scherer equation^[37]:

$$D = B\lambda / \beta_{1/2} \cos\theta$$

where D is the average crystallite size of the phase under investigation, B is the Scherer constant (0.89), λ is the wavelength of the X-ray beam used (1.54056 Å), $\beta_{1/2}$ is the full width at half maximum (FWHM) of diffraction peak and θ is

the diffraction angle. The calculation of the crystallite size by the Scherer formula was created and based on the first two peaks with (003) and (006) plane that characterize the hydroxalcalite compound.

The crystallite size in both a and c directions decreased due to the presence of ultrasound treatment compared to the crystallite size for Mg–Al LDH_{s1} prepared at constant -pH without sonication.

Table 1: Structural parameters of LDH crystallines prepared using different methods.

Properties	Methods	
	without sonication	under sonication
Basal spacing (d_{006})Å	7.65	8.766
d_{006} (Å)	4.321	4.383
d_{009} (Å)	2.572	2.581
d_{110} (Å)	1.534	1.532
Lattice parameter ^a , a(Å)	3.068	3.064
Lattice parameter ^b , c(Å)	22.95	26.298
Crystallite size ^c (nm)	26.00	5.00

$$^a a = 2d_{110}$$

$$^b c = 3d_{003}$$

^cValue calculated from the Scherrer equation

The lattice parameters $a = 2d_{006}$ (cation–cation distance in the brucite-like layer) and $c = 3d_{003}$ (thickness of one brucite-like layer and one interlayer) were calculated (Table 1). The parameter a ($a = 3.06$ Å) was the same and essentially independent of the synthesis method of Mg–Al LDH_s. As for the lattice parameter c, it corresponds to the 3 layers rhombohedra polytype 3R^[38]. The resulting interlayer distance $d_{003} = c/3$ depends on the layer charge density, the nature of the interlayer anion (CO₃²⁻) and the number of water molecules in the interlayer space.

The basal spacing, which corresponding to the d value of the 003 diffraction peak in the pattern, for the sample prepared under ultrasound treatment is $c/3 = 8.766$ Å, very much larger than the value reported for Mg–Al hydroxalcalite prepared by conventional method without ultrasound treatment with what is expected for the intercalated carbonates^[38] setting in D_{3h} orientation with the 3-fold axis being parallel to the c-direction ($d_{003} = 7.65$ Å at constant pH). This increase of the basal spacing related to the c parameter can be explicated by a different orientation of the lactate anion in the interlayer spacing that the stacking arrangement existing in the intercalated carbonate anion may be improved by the presence of ultrasound treatment, also causing a lowering of symmetry of carbonate anion of D_{3h} to C_{3v} symmetry. The interlayer region hosts the carbonate counter anions and water molecules that are placed in the intermediate plane between two adjacent sheets.

Regarding the sample prepared at constant pH without sonication, the structure of the studied phase was refined as isotopic to the rhombohedra hydroxalcalite [Mg_{0.64}Al_{0.36}(OH)₂](CO₃)_{3/0.18}·0.46H₂O^[35]. The structure refinement was initiated by building octahedral coordination for metallic cations. The metals (Mg and Al) were distributed in the 3a (0, 0, 0) site of the $R\bar{3}m$ space group. Accordingly, one constraint, namely N (Co) + N (Al) = 1 was satisfied, i.e. 3a sites were totally occupied by Mg and Al cations.

The oxygen atoms of hydroxyl groups are located in particular positions 6c (0, 0, z). As regards the carbon atoms of the carbonate groups in the interlayer domain species, they are located in 6c (1/3, 2/3, 0.5) positions. Besides, the oxygen atoms of the water molecules and those of the carbonate groups are all located in position 18h (x, -x, 0.5).

The final refinement included the scale factor, profile shape and atomic parameters (positions, occupancies, and isotropic thermal displacements). The following good agreement factors are $R_B = 5.2\%$ and $R_F = 3.50\%$. The results of refinement are given in Table 2 and the corresponding X-Ray diffraction pattern is shown in (Figure.2). The formula assigned to the compound must be $Mg_{0.74(4)}Al_{0.26(3)}(OH)_2(CO_3)_{0.13(2)}(H_2O)_{0.397(5)}$. This composition corresponds to an Mg/Al ratio 3 that is identical to the initial mixture stoichiometry (0.75 / 0.25).

Table 2: Positional, occupancy and thermal parameters with their standard deviations after Rietveld refinement of Co-Al-Co₃ LDH $Mg_{0.74(4)}Al_{0.26(3)}(OH)_2(CO_3)_{0.13(2)}(H_2O)_{0.397(5)}$ in the $R\bar{3}m$ space group.

Atom	Site	Occupancy	x	y	z	$\beta(\text{\AA}^2)$
Mg	3a	0.732(4)	0	0	0	1.270(3)
Al	3a	0.262(5)	0	0	0	1.270(3)
O(1)	6c	1.000(0)	0	0	.370(2)	1.875(3)
H(1)	6c	1.000(0)	0	0	.418(0)	2.400(0)
C	6c	0.031(8)	1/3	2/3	0.51	1.490(4)
O(2)	18h	0.119(6)	0.155(3)	-0.155(3)	0.5	1.360(2)

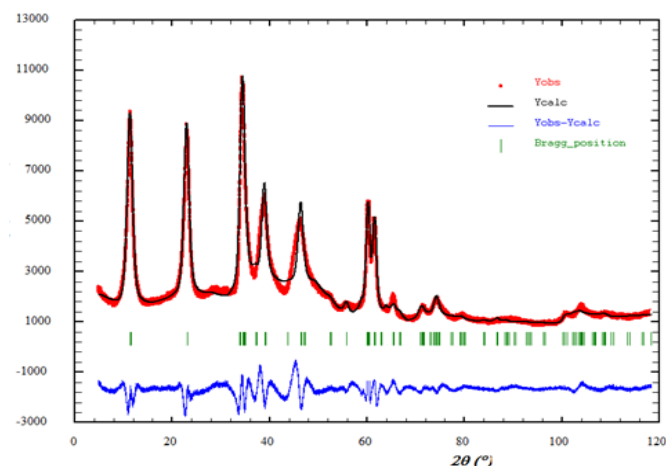


Figure-2: The X-ray diffraction pattern and the final Rietveld refinement plot of the Mg-Al-CO₃ LDH_{S1}. Points correspond to experimental values, and the continuous lines represent the calculated pattern; vertical bars indicate the positions of Bragg peaks. The bottom trace depicts the difference between the experimental and the calculated intensity values.

Spectroscopic analysis

The IR spectra of the two samples prepared without and under sonication are reported in (Figure.3). Each spectrum resembles those of other hydroxalite-like phases^[18,38]. Typical for these spectra are the strong broad absorbance band vibration between 3000 and 3600 cm⁻¹ at around 3390 cm⁻¹ which are associated with OH-stretching vibrations from OH groups as well as interlayer water molecules.

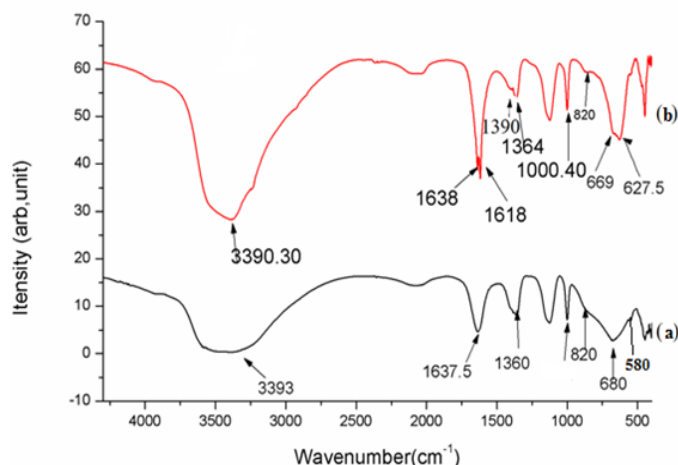


Figure-3: (a) Infrared spectrum of Mg-Al-CO₃ LDH prepared without Ultrasound treatment (b) Infrared spectrum of Mg-Al-CO₃ LDH prepared under Ultrasound treatment.

As for the sample prepared without ultrasound treatment, the bands in the range 400 - 900 cm⁻¹ provide evidence that the characteristic LDH network has been formed. The absorption band at 450 cm⁻¹ is due to the O-Al-O deformation mode (δ_{O-Al-O}), while those at 580 cm⁻¹ correspond to Al-O stretching vibrations (ν_{O-Al-O})^[39,40]. The strong band observed at 1637.5 cm⁻¹ corresponds to the H-O-H deformation mode of intercalated water molecules ($\delta_{(H_2O)}$). The strong bands observed respectively at 1360 cm⁻¹ and 820 cm⁻¹ can be attributed to the anti-symmetric stretching mode ν_3 and the anti symmetric bending mode ν_2 of CO₃ groups, respectively. Moreover, the symmetric ν_4 (CO₃²⁻) bending mode was observed at 611 cm⁻¹ which corresponds to intercalated CO₃²⁻ in D_{3h} symmetry^[41,42].

Concerning the sample prepared under ultrasound treatment, the two vibration bands at around 1618 and 1638 cm⁻¹ are assigned, respectively, to the stretching vibrations and deformation of water molecules intercalated in the interlayer space. To our knowledge, a single band on the deformation mode ($\delta_{(H_2O)}$) has been reported to LDH prepared by conventional coprecipitation without sonication^[41-44]. The appearance of two bands can be explained by the fact the ultrasound irradiation, also causing a lowering of symmetry of carbonate anion of D_{3h} to C_{3v} and we know that the oxygen atoms of water molecules and those of carbonates groups are located in same position in the interlayer spacing, this lowering of symmetry leads to formation of two, not equivalents groups of water molecule in the interlayer space, or one of two groups are assigned by the vibration bands at around 1618 cm⁻¹ and the other groups of water molecule are assigned by a vibration band at around 1638 cm⁻¹. The unperturbed carbonate ion is a planar triangle with point symmetry D_{3h}. The free ion, CO₃²⁻ with D_{3h} symmetry exhibits four normal vibrational modes: (I) asymmetric stretching vibration (ν_1), (II) an out-of-plane bend (ν_2), (III) a doubly degenerate asymmetric stretch (ν_3), and (IV) a doubly degenerate bending mode (ν_4).

The symmetries of these modes are A₁' (R) + A₂' (IR) + E' (R, IR) + E'' (R, IR) and Occur at 1063, 879, 1415 and 680 cm⁻¹, respectively. It can also be noted the presence of the IR active absorption band arising from the carbonate anion observed at 1360 - 1390 cm⁻¹ (ν_3), 800 cm⁻¹ (ν_2) and 628 - 670 cm⁻¹ (ν_4) providing evidence in this case, for the sample prepared under ultrasound treatment. The two bands observed in the spectra of

the sample, prepared under ultrasound treatment in the region $1360 - 1390 \text{ cm}^{-1}$, can be attributed either to the disordered nature of the interlayer or to a lowering of the symmetry of the carbonate anions from D_{3h} to C_{3v} in the interlayer, which lifts the degeneracy of the ν_3 mode. Moreover, the vibration band ν_4 (CO_3^{2-}) which currency in two new bands at 628 and 669 cm^{-1} well confirms this decline of symmetry that lifts the degeneracy of the ν_4 mode. The ν_1 mode (CO_3^{2-}) is usually inactive in infrared spectroscopy when carbonate anions are in symmetry D_{3h} . The appearance of this band at about 1000 cm^{-1} suggests a lowering of symmetry for the carbonate ion of D_{3h} to C_{3v} [37,38].

The infrared absorption spectrum of the compound prepared under sonication confirming the results of structural studies by X-ray diffraction of this compound, such that the increase of the interlayer distance and thereafter the parameter c was expressed by the lowering of symmetry of the carbonate ion (D_{3h} to C_{3v}) and the presence of two types of water molecules in the interlayer spacing.

The thermal decomposition of Mg-Al- HTLcs

Differential thermal and thermo gravimetric analysis

The thermal decomposition of the prepared synthetic Mg-Al-LDH_{s1} compound was investigated by TGA-DTA analysis. According to the literature [18-45] the thermal decomposition of LDHs includes three main stages which are the loss of adsorbed water, the decomposition of structural hydroxyl groups, and finally the decomposition of interlayer carbonate anions.

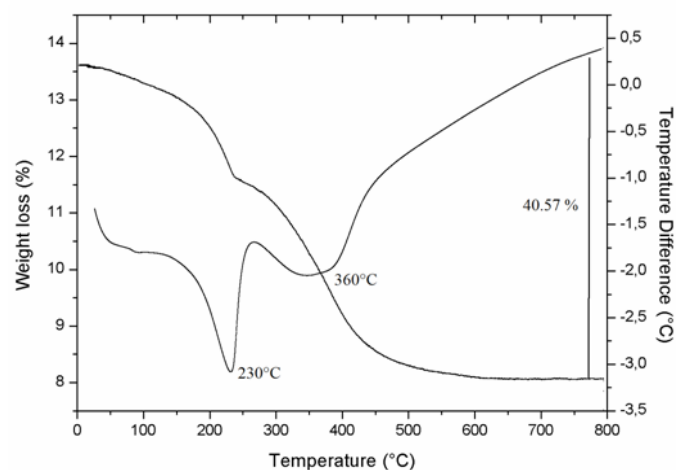


Figure 4: Thermal analysis curves (TGA/DTA) of Mg-Al- CO_3 LDH_{s1}.

The Thermal Analysis Curves (TGA/DTA) of the prepared LDH, displayed in Figure 4, are quite similar to those obtained and reported in previous research works [46]. The TGA curve is characterized by a continuous mass loss without well-defined plateaux between the decomposition steps. The first mass loss of 2% at 50°C , corresponding to a broad endothermic peak, can be accredited to the loss of adsorbed water. It is followed by a second more pronounced and sharp endothermic phenomenon, around 230°C and corresponding to 14.5% of the total mass, due to the loss of hydration water from the interlayer region (decomposition of structural hydroxyl groups). A third step, extending up to 430°C and corresponding to 40.57% of the total mass, is assigned to the overlapped mass losses due to the dehydroxylation of the layers and the decomposition of the carbonates

counter-anions as carbon dioxide. It is associated with a broad endothermic peak at 360°C . With respect to the TGA analysis, the Mg-Al- CO_3 LDH exhibits a total mass loss of 40, 57%. After decomposition at 550°C , the solid product is composed of a spinel oxide phase (MgAl_2O_4) and MgO oxide compound.

Heating in the Raman microscope

In general, two essential stages can be observed during phase transformation of LDHs upon heating: (i) a shift of LDH basal spacing associated with the release of interlayer water and (ii) the disappearing of the LDH diffraction lines and the formation of oxides phases. This result confirmed by TGA analysis can also be confirmed by Heating in the Raman microscope for the synthetic hydrotalcite, $\text{Mg}_{0,74(4)}\text{Al}_{0,26(3)}(\text{OH})_2(\text{CO}_3)_{0,13(2)}(\text{H}_2\text{O})_{0,397(5)}$. Figure 5 reveals the Raman spectra of this sample recorded at room temperature, the strong bands around 553 cm^{-1} are assigned before as the M–OH translation and deformation modes of the hydroxide layers. The presence of carbonate, CO_3^{2-} is reflected by the relatively broad and weak bands around 1058 cm^{-1} (ν_1 (CO_3^{2-})) and 1224 cm^{-1} (ν_3 (CO_3^{2-})). The weak band at around 1670 cm^{-1} is assigned to the deformation mode of the interlayer water molecules $\delta_{(\text{H}_2\text{O})}$. Figure 6 shows the effects of heating from 50°C to 600°C on the Raman spectra of synthetic hydrotalcite, $\text{Mg}_{0,74(4)}\text{Al}_{0,26(3)}(\text{OH})_2(\text{CO}_3)_{0,13(2)}(\text{H}_2\text{O})_{0,397(5)}$.

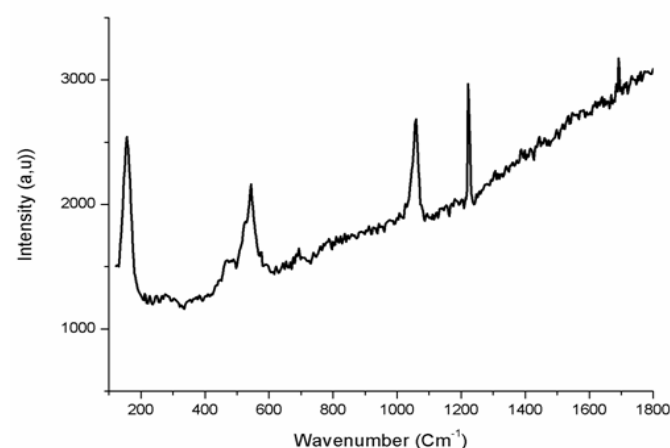


Figure 5: The Raman spectra of Mg-Al- CO_3 LDH_{s1} recorded at room temperature.

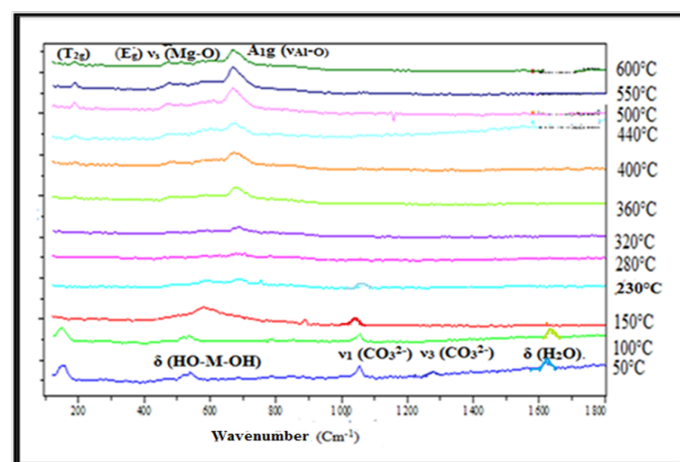


Figure 6: The Raman spectra of Mg-Al- CO_3 LDH_{s1} heating from 50°C to 600°C .

At 50°C, (Figure 7a) displays that the presence of the strong bands around 553 cm⁻¹ is assigned to the M–OH translation and deformation modes of the hydroxide layers. These bands strongly decrease in intensity upon heating; they disappear above 150°C. The intensities of these two bands, attributed to the presence of carbonate anion (ν_1 and ν_3 mode), do not show significant changes upon heating to approximately 100°C. Although the bands become better visible due to a decrease in intensity ν_1 and ν_3 disappear around 230 – 320 °C while a new band becomes visible around 700 cm⁻¹ up to 360°C, can be reasonably considered as arising from the A_{1g} symmetry mode which is usually ascribed to the stretching vibrations of oxygen atoms inside the octahedral BO₆ unit corresponding to the Al–O stretching vibration ($\nu_{\text{Al-O}}$) of octahedral AlO₆ of MgAl₂O₄ like-spinel^[47,48]. The strong band observed at 480 cm⁻¹ is thought to be due to E_g symmetry Mg–O stretching vibrations ($\nu_{\text{Mg-O}}$) and the line around 191 cm⁻¹ is assigned to the lowest frequency T_{2g} symmetry species corresponding to the (Mg,Al)–O bending vibration ($\delta_{(\text{Mg,Al})\text{-O}}$) in the tetrahedral A site for MgAl₂O₄ like-spinel^[47,48]. This behavior is in good agreement with the TGA/DTA pattern where dehydroxylation and decarbonisation of the hydroxalite structure start above 230°C.

The minor band around 1670 cm⁻¹ assigned to the deformation mode of water appears from room temperature to 50°C ; upon heating, this band disappears above 100°C attributed to dehydration. The relatively high frequency of 1670 cm⁻¹ suggests that this band is associated with the interlayer water assigned to the increasing movement of the water molecules in the interlayer upon heating, The Raman signal becomes weaker and finally unobservable above 100°C. This behavior is in good agreement with the TGA/DTA pattern where dehydration of the interlayer region started at above 50°C and finished at around 230°C. Increasing calcinations temperature enhanced the crystallization of MgO- like phase and, additionally, MgAl₂O₄ spinel was detected in the samples heated from 500 to 600 °C.

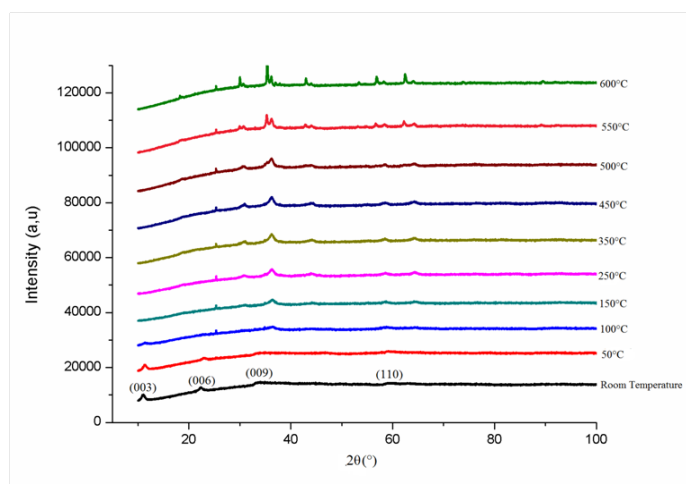


Figure 7: XRD patterns of Mg-Al-CO₃ LDH_{s1} in the range from room temperature to 600°C.

In situ variable temperature XRD analysis

Figure 7 shows *in situ* HT-XRD patterns in the range from room temperature to 600 °C of samples obtained without ultrasound irradiation. The studied transformations involve changes in the sample composition, in particular as regards water and interlamellar carbonates groups. With increasing tem-

perature up to 100°C, the position of the (003) reflection shifts to higher angle indicating a decrease in interlayer spacing. The heating causes a displacement of the diffraction lines (001) to large angles and changes of their intensities. The gradual decline of the ratio of intensities of the lines (006) and (003), from room temperature to 100°C, is associated with the elimination of physisorbed and interlayer water and the loss of hydrogen bonding without collapse of the layered structure.

Indeed, the elimination of water molecules causes a reduction of the electron density and, consequently, the reduction of the intensities of the diffraction lines relating to diffraction planes types (001). Between 100 and 350°C, a contraction of the interlamellar distance and partial decarbonation is produced. This gives rise to an increase in intensity and a shift to the high angles of the diffraction lines (001) connected to the stacking sequence of the layers. The line (003) from 11.4 ° (7.56 Å) to 12.0 ° (6.91 Å), the line (006) 22.9 ° (3.88 Å) to 27.4 ° (3.26 Å) and the line (009) 33.6 ° to 38.9 °. From this contraction of the interlamellar distance corresponds to the end of dehydration phenomenon and partial decarbonisation of summer slip started by the loss of a portion of the anions intercalated carbonates reflecting the creation of a partial disorder of the structure. In the temperature range 350 - 600°C, the diffraction lines of the HDL-phase disappear and new lines corresponding to new phases, weakly crystallized, appear. They are the kind MgO oxide phase and the spinel phase MgAl₂O₄. From 550°C, oxides obtained are better crystallized.

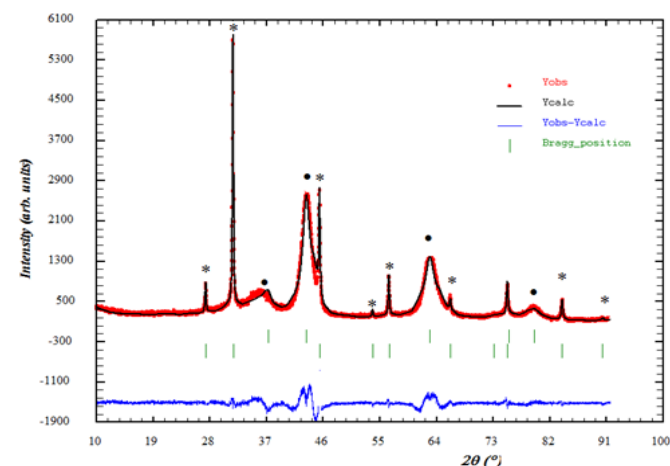


Figure 8: The X-Ray diffraction pattern and the final Rietveld refinement plot for the mixture oxides product obtained after decomposition of the Mg-Al-CO₃ LDH_{s1} at 600°C. Points correspond to experimental values, and the continuous lines represent the calculated pattern ; vertical bars indicate the positions of Bragg peaks. The bottom trace depicts the difference between the experimental and the calculated intensity values.

• Corresponds to the MgO phase, *Correspond to the spinel phase MgAl₂O₄.

Rietveld refinement of the powder diffraction X-ray chart of HDL decomposition product calcined at 600°C was achieved. Above 600°C, the characteristic peaks of mixed metal oxides are apparent; a mixture of spinel MgAl₂O₄ and MgO phase's evolves. This result is confirmed by the rietveld refinement of the sample calcined at 600°C. Figure 8 presents the experimental and refined X-Ray diffraction pattern and their differences for the sample calcined at 600°C. Rietveld refinement

in profile matching results revealed a mixture of two phases: periclase cubic MgO (35%) phase with refined cell parameter $a = 4.127(3) \text{ \AA}$ in space group and spinel-like phase MgAl_2O_4 (65%) with refined cell parameter $a = 8.355(2) \text{ \AA}$, space group. This can indicate that after the decomposition of the hydrotalcite phase, aluminum tends to remain in a mixed oxide phase, while the MgO structure (periclase or rock-salt) has the same oxygen packing of MgAl_2O_4 spinel (cubic close packing), the percentage of each phase was calculated by the quantitative phase analysis with the Reference Intensity Ratio (RIR) method^[49].

Adsorption of fluoride

Figure 9 shows that the best efficiency of defluoridation is obtained with the compound prepared under ultrasound treatment, corresponding to an amount of fluoride absorbed equal to 91.55 mg / g of sample. It is 64.6% for the Mg-Al HDL calcined at 600°C and 61.9% in HDL prepared without sonication. Besides, the saturation time (50 minutes) is significantly less for the sample prepared under sonication than for the sample calcined at 600 °C (150 min) and than for the HDL prepared by conventional method (170 min). This result indicates that a higher basal spacing and smaller crystallites size of hydrotalcite compound favor the fluoride removal in contaminated water.

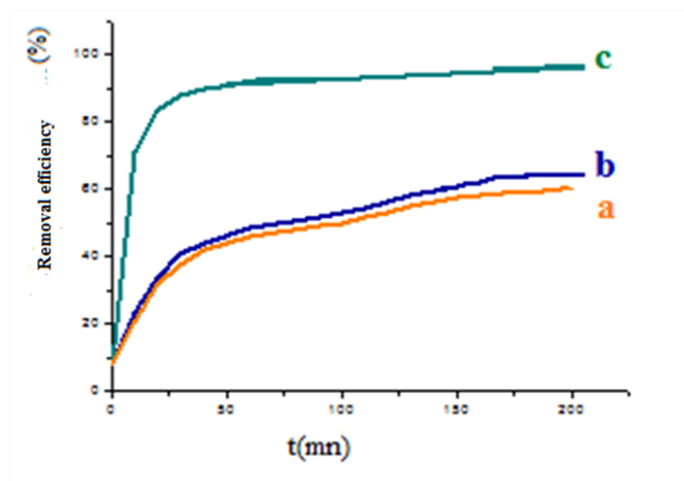


Figure 9: Measurement of the removal efficiency (E) of fluoride ion in function of time for: (a) HDL prepared without sonication, (b) product calcined at 600°C. (c) HDL prepared under sonication.

Conclusion

Mg-Al hydrotalcite-like compounds were synthesized by the coprecipitation method and under ultrasound treatment. The ultrasound treatment has a clear influence not only on the structural, textural and chemical properties of the produced LDH minerals, but also on the fluoride removal properties. Besides, the ultrasound treatment can cause an increase in basal spacing and a decrease in crystallites size compared to the sample prepared without ultrasound treatment. From the present study, it can be seen that the ultrasound treatment can be used effectively for the removal of the fluoride anions from aqueous solutions.

The crystallographic formula shown for the sample prepared without ultrasound treatment after Rietveld refinement is $[\text{Mg}_{0.74(4)}\text{Al}_{0.26(3)}(\text{OH})_2(\text{CO}_3)_{0.13(2)}(\text{H}_2\text{O})_{0.397(5)}]$. Heating stages Raman microscopy for this sample were shown, in this paper, to be a very useful tool to study the structural changes and re-

actions like dehydration, dehydroxylation and decarbonisation in crystalline materials like hydrotalcites. During heat treatment along with the conventional techniques as XRD and TGA/DTA. Further heating up to 600°C dehydroxylation is generally completed and new phases, including spinel (MgAl_2O_4) and MgO are formed. This result can be confirmed by the rietveld refinement of a sample calcined at 600°C.

Acknowledgments

The authors are particularly grateful to Professor Mr. Alain Bulou (LUMAN Université, Université du Maine, CNRS UMR 6283, Institut des Molécules et Matériaux du Mans (IMMM)) for performing Raman and Infrared measurements. The authors wish to express their gratitude to M. Wassim Hriz from the Faculty of Science, Sfax, Tunisia for his valuable proofreading and language polishing services.

References:

- Rives, V., Ulibarri, M. A. Layered double hydroxides (LDH) intercalated with metal coordination compound and oxometalates. (1999) *Coordination Chem Rev* 181(1): 61-120.
[Pubmed](#) | [Crossref](#) | [Others](#)
- Rives, V. Characterisation of Layered double hydroxides and of their decomposition products. (2002) *Materials Chemistry and Physics* 75(1-3): 19-25.
[Pubmed](#) | [Crossref](#) | [Others](#)
- Trifiro, F., Vaccari, A., Davies, J. E. D., et al. Bein, Hydrotalcite-like Anionic Clays (Layered double hydroxides). (1996) *Solid-State Supramolecular Chemistry* 7: 251-291.
[Pubmed](#) | [Crossref](#) | [Others](#)
- Cavani, F., Trifiro, F., Vaccari, A. Hydrotalcite-type anionic clay: Preparation, properties and application. (1991) *Catalysis Today* 11(2): 173-301.
[Pubmed](#) | [Crossref](#) | [Others](#)
- Nakagaki, Sh., Halma, M., Bail, A., et al. First insight into catalytic activity of anionic iron porphyrins immobilized on exfoliated layered double hydroxides. (2005) *J Colloid and Interface Sci.* 281(2): 417-423
[Pubmed](#) | [Crossref](#) | [Others](#)
- Wang, S. L., Hseu, R.J., Chang, R.R., et al. Adsorption and Thermal Desorption of Cr (VI) on Li/ Al Layered Double Hydroxide. (2006) *Colloids Surf* 277(1-3): 8–14.
[Pubmed](#) | [Crossref](#) | [Others](#)
- Lazaridis, N.K., Pandi, T.A., Matis, K.A. Chromium (VI) Removal from Aqueous Solution by Mg-Al-CO₃ Hydrotalcite: Sorption-Desorption Kinetic and Equilibrium Studies. (2004) *Ind Eng Chem Res* 43(9): 2209-2215.
[Pubmed](#) | [Crossref](#) | [Others](#)
- Choy, J.H., Choi, S. J., Oh, J.M., et al. Clay minerals and layered double hydroxides for novel biological application. (2007) *Applied Clay science* 36(1-3): 122-132.
[Pubmed](#) | [Crossref](#) | [Others](#)
- Mandal, S., Mayadevi, S. “Fluoride contamination of water: Remediation by adsorption” Book chapter in “Fluoride: Properties, Applications and Environmental Management”. (2011) Nova Science Publishers 40: 159-176.
[Pubmed](#) | [Crossref](#) | [Others](#)
- Hansen, H. C. B., Koch C. B. Synthesis and characterization of pyroaurite. (1995) *Applied Clay Science* 10(1-2): 5-9.
[Pubmed](#) | [Crossref](#) | [Others](#)
- Bellotto, M., Rebours, B., Clause, O., et al. A Reexamination of Hydrotalcite Crystal Chemistry. (1996) *J Phys Chem* 100(20): 8527-8534.
[Pubmed](#) | [Crossref](#) | [Others](#)
- Oh, J. M., Hwang, S. H., Choy, J. H. The effect of synthetic conditions on tailoring the size of hydrotalcite particles. (2002) *Solid State Ionics* 151(1-4): 285-291.
[Pubmed](#) | [Crossref](#) | [Others](#)
- Saiah, F.B.D., Lian Su, B. N., Bettahar, B. Nickel-iron layered double hydroxides (LDH) Textural properties upon hydrothermal treatments and applications on dye sorption. (2009) *Journal of Hazardous Materials* 165(1-3): 206-217.
[Pubmed](#) | [Crossref](#) | [Others](#)
- Coronado, E., Galán-Mascaros, J.R., Gastaldo, C.M., et al. Spontaneous magnetization in Ni-Al and Ni-Fe layered double hydroxides. (2008) *Inorg Chem* 47(19): 9103-9110.
[Pubmed](#) | [Crossref](#) | [Others](#)
- Bravo-Suarez, J. J., Paez-Mozo, E. A., Oyama, S. T. Review of the synthesis of layered double hydroxides : a thermodynamic approach. (2004) *Quimica Nova* 27(4): 601-614.
[Pubmed](#) | [Crossref](#) | [Others](#)
- Benito, P., Guinea, I., Herrero, M., et al. Incidence of microwave hydrothermal treatments on the crystallinity properties of hydrotalcite-like compounds. (2007) *Anorg Allg Chem* 633(11-12): 1815-1819.
[Pubmed](#) | [Crossref](#) | [Others](#)
- Zhao, H., Nagy, k. L. Dodecyl sulfate-hydrotalcite nanocomposites for trapping chlorinated organic pollutants in water. (2004) *J Colloid Interface Sci* 274(2): 613-624.
[Pubmed](#) | [Crossref](#) | [Others](#)
- Babay, S., Bulou, A., Mercier, A. M., et al. The decomposition of the layered double hydroxides of Co and Al: Phase segregation of a new single phase spinel oxide. (2015) *Spectrochim Acta A Mol Biomol Spectrosc* 15(141): 80-87.
[Pubmed](#) | [Crossref](#) | [Others](#)
- A.J. Marchi., J.I. Di Cosimo., C.R. Apesteguia. Influence of chemical composition on the preparation of Cu-Co-Zn-Al mixed oxide catalysts with a high metal dispersion. (1993) *Stud Surf Cat* 75: 1771-1774.
[Pubmed](#) | [Crossref](#) | [Others](#)
- Salomão, R., Milena, L. M., Wakamatsu, M. H., et al. Hydrotalcite synthesis via co-precipitation reactions using MgO and Al (OH)₃ precursors. (2011) *ceramics international* 37(8): 3063-3070.
[Pubmed](#) | [Crossref](#) | [Others](#)
- LakrAIMI, M., Legrouri, A., Barroug, A., et al. Preparation of a new stable hybrid material by chloride–2,4-dichlorophenoxyacetate ion exchange into the zinc–aluminum–chloride layered double hydroxide. (2000) *Journal of Materials Chemistry* 10: 1007-1011.
[Pubmed](#) | [Crossref](#) | [Others](#)
- Islam, M., Patel R. Nitrate sorption by thermally activated Mg/Al chloride hydrotalcite-like compound. (2009) *J Hazard Mater* 169(1-3): 524-531.
[Pubmed](#) | [Crossref](#) | [Others](#)
- Geraud, E., Bouhent, M., Derriche, Z., et al. Texture Effect of Layered Double Hydroxides on Chemisorption of Orange II. (2007) *Journal of physics and chemistry of solids* 68(5-6): 818-823.
[Pubmed](#) | [Crossref](#) | [Others](#)
- D.P. Das., J. Das., K. Parida. Physicochemical characterization and adsorption behavior of calcined Zn/Al hydrotalcite-like compound (HTlc) towards removal of fluoride from aqueous solution. (2003) *J Colloid Interface Sci* 261(2): 213–220.
[Pubmed](#) | [Crossref](#) | [Others](#)
- Gaini, E., LakrAIMI, L., Sebbar, M., et al. Removal of Indigo Carmine Dye from Water to Mg-Al-CO₃- calcined Layered Double hydroxides. (2009) *J Hazard Mater* 161(2-3): 627–632.
[Pubmed](#) | [Crossref](#) | [Others](#)
- Lv, L., He, J., Wei, M., et al. Uptake of chloride ion from aqueous solution by calcined layered double hydroxides: equilibrium and kinetic studies. (2006) *Water Res* 40(4): 735-743.
[Pubmed](#) | [Crossref](#) | [Others](#)
- Ensar, O. Adsorption of fluoride on gas concrete materials. (2005) *J Hazard Mater* 117(2-3): 227–233.
[Pubmed](#) | [Crossref](#) | [Others](#)
- Reardon, E.J., Wang, Y. A limestone reactor for fluoride removal from waste waters Environ. (2000) *Sci Technol* 34(15): 3247–3253.
[Pubmed](#) | [Crossref](#) | [Others](#)
- Amor, Z., Malki, S., Taky, M., et al. Optimization of fluoride removal from brackish water by electro dialysis. (1998) *Desalination* 120(3): 263–271.
[Pubmed](#) | [Crossref](#) | [Others](#)
- Mandal, S., Patil, V.S., Mayadevi, S. Alginate and hydrotalcite-like anionic clay composite systems: Synthesis, Characterization and Application Studies. (2012) *Microporous and Mesoporous Materials* 158: 241-246.
[Pubmed](#) | [Crossref](#) | [Others](#)
- Biswas, K., Gupta K., Goswami, A., et al. Fluoride removal efficiency from aqueous solution by synthetic iron(III)-aluminum(III)-chromium(III) ternary mixed oxide. (2010) *Desalination* 255(1-3): 44-51.
[Pubmed](#) | [Crossref](#) | [Others](#)
- Yang, M., Hashimoto, T., Hoshi, N., et al. Fluoride removal in a fixed bed packed with granular calcite. (1999) *Water Research* 33(16): 3395-3402.
[Pubmed](#) | [Crossref](#) | [Others](#)

33. Castel, C., Schweizer, M., Simonnot, M.O., et al. Selective removal of fluoride ions by a two way Ion exchange cyclic process. (2000) *Chem Eng Sci* 55(17): 3341-3352.
[Pubmed](#) | [Crossref](#) | [Others](#)
34. Amor, Z., Bariou, B., Mameri, N., et al. Fluoride removal from brackish water by electrodialysis. (2001) *Desalination* 133(3): 215-223.
[Pubmed](#) | [Crossref](#) | [Others](#)
35. Rodriguez-Carvajal, J. “Programme FULLPROF “. (2005) version 2.6.1
[Pubmed](#) | [Crossref](#) | [Others](#)
36. Roisnel, T., Rodriguez-Carvajal, J. WinPLOTR: A Windows tool for powder diffraction pattern analysis. (2001) *J Mater Sci Forum* 378(1-2): 118-123.
[Pubmed](#) | [Crossref](#) | [Others](#)
37. Koch, C.C. The Synthesis of Non-Equilibrium Structures by Ball-Milling. (1992) *Materials Science Forum* (88-90): 243-262.
[Pubmed](#) | [Crossref](#) | [Others](#)
38. Costantino, U., Nocchetti, M., Marmottini, F., et al. New synthetic route to hydrotalcite-like compounds: characterisation and properties of the obtained materials. (1998) *Eur J Inorg Chem* 1439-1446.
[Pubmed](#) | [Crossref](#) | [Others](#)
39. Lagadic, I., Leautic, A., Clement, R. Intercalation of polyether's into the MPS3 (M = Mn, Cd) host lattice. (1992) *Journal of the Chemistry Society, Chemical Communication* 19: 1396-1397.
[Pubmed](#) | [Crossref](#) | [Others](#)
40. Li, F., Zhang, L. H., Evans, D. G., et al. The calcined LDHs were submitted to X-ray photoelectron spectroscopy, *Colloids Surf. (2004) A: Physicochem. Eng. Aspects.* 244: 169-177.
[Pubmed](#) | [Crossref](#) | [Others](#)
41. Frost, R.L., Jagannadha Reddy, B. Thermo-Raman spectroscopic study of the natural layered double hydroxide manasseite. (2006) *Spectrochim Acta Part a Mol Biomol Spectrosc* 65(3-4): 553–559.
[Pubmed](#) | [Crossref](#) | [Others](#)
42. Bernal, M.E.P., Casero, R.J.R., Rives, V. Preparation and properties of Co-Fe mixed oxides obtained by calcination of layered doubles hydroxides. (2004) *Ceramics Silikaty* 48(4): 145-154.
[Pubmed](#) | [Crossref](#) | [Others](#)
43. Montanari, T., Sisani, M., Nocchetti, M., et al. Layered double hydroxides and their intercalation compounds in photochemistry and in medicinal chemistry. (2009) *Catalysis Today* 25: 6425-6431.
[Pubmed](#) | [Crossref](#) | [Others](#)
44. Klopogge, J.T., Hockey, L., Frost, R.L. The effects of synthesis pH and hydrothermal treatment on the formation of zinc aluminum hydroxaltes. (2004) *J Solid State Chem* 177(11): 4047-4057.
[Pubmed](#) | [Crossref](#) | [Others](#)
45. Rozov, K., Berner, U., Taviot-Gueho, C., et al. Synthesis and characterization of the LDH hydrotalcite-pyroaurite solid-solution series. (2010) *Cement and Concrete Research* 40(8): 1248-1254.
[Pubmed](#) | [Crossref](#) | [Others](#)
46. Yan, K., Xi, X., Li, J., et al. Preparation, Characterization, and Catalytical Application of MgCoAl-Hydrotalcite-Like Compounds. (2007) *Nat Gas Chem* 16(4): 371–376.
[Pubmed](#) | [Crossref](#) | [Others](#)
47. Ohoro, M.P., Frisillo, A. L., White, W. B. Lattice Vibrations of MgAl₂O₄ Spinel. (1973) *J Phy Chem Solids* 34(1): 23-28.
[Pubmed](#) | [Crossref](#) | [Others](#)
48. Lemański, K., Dereń, P.J., Walerczyk, W., et al. Spectroscopic and structural properties of MgAl₂O₄:Nd³⁺ nanopowders and ceramics. (2014) *Journal of Rare Earths* 32(3): 265-268.
[Pubmed](#) | [Crossref](#) | [Others](#)
49. Chung, F.H. Quantitative interpretation of X-ray diffraction patterns of mixtures I. Matrix-flushing method for quantitative multi component analysis. (1974) *J Appl Crystallogr* 7: 519-525.
[Pubmed](#) | [Crossref](#) | [Others](#)